The tumor suppressor RASSF1A modulates inflammation and injury in the reperfused murine myocardium

Received for publication, April 18, 2019, and in revised form, July 11, 2019 Published, Papers in Press, July 16, 2019, DOI 10.1074/jbc.RA119.008970

Jamie Francisco[1], **Jaemin Byun**[1], **Yu Zhang, Olivia Berman Kalloo, Wataru Mizushima, Shinichi Oka, Peiyong Zhai, Junichi Sadoshima, and Dominic P. Del Re**[2]

From the Department of Cell Biology and Molecular Medicine, Cardiovascular Research Institute, New Jersey Medical School, Rutgers University, Newark, New Jersey 07103

Edited by Roger J. Colbran

Inflammation is a central feature of cardiovascular disease, including myocardial infarction and heart failure. Reperfusion of the ischemic myocardium triggers a complex inflammatory response that can exacerbate injury and worsen heart function, as well as prevent myocardial rupture and mediate wound healing. Therefore, a more complete understanding of this process could contribute to interventions that properly balance inflammatory responses for improved outcomes. In this study, we leveraged several approaches, including global and regional ischemia/reperfusion (I/R), genetically modified mice, and primary cell culture, to investigate the cell type–specific function of the tumor suppressor Ras association domain family member 1 isoform A (RASSF1A) in cardiac inflammation. Our results revealed that genetic inhibition of RASSF1A in cardiomyocytes affords cardioprotection, whereas myeloid-specific deletion of RASSF1A exacerbates inflammation and injury caused by I/R in mice. Cell-based studies revealed that RASSF1A negatively regulates NF-κB and thereby attenuates inflammatory cytokine expression. These findings indicate that myeloid RASSF1A antagonizes I/R-induced myocardial inflammation and suggest that RASSF1A may be a promising target in immunomodulatory therapy for the management of acute heart injury.

Aberrant inflammation is thought to underlie a host of pathologies, including those related to cardiovascular disease such as atherosclerosis, injury caused by myocardial infarction (MI),[3] and the progression to heart failure (1). Ischemia, either accompanied by reperfusion (I/R) or not, elicits massive cardiomyocyte loss. Damage-associated molecular patterns released from dead cells trigger robust activation of the innate immune response, which is associated with adverse clinical outcomes (2–4). Although a balanced inflammatory reaction is necessary for optimal wound healing, prolonged inflammation can exert deleterious effects within the myocardium leading to greater cardiomyocyte loss, increased fibrosis, and worsened heart function (4, 5). Moreover, efforts to attenuate this response have shown therapeutic promise in mouse MI models (6, 7). To date, results from clinical trials targeting inflammation have been inconclusive (8–10). Importantly, the molecular mechanisms that modulate cardiac inflammation remain incompletely understood, representing a potential barrier to improved therapeutics for patients suffering MI.

Ras association domain family member 1 isoform A (RASSF1A) is a tumor suppressor and protein scaffold that lacks catalytic activity and regulates signaling through protein interactions (11). Loss of RASSF1A function, either through point mutations or epigenetic silencing, is observed with high frequency in multiple tumor types (12). However, its role in heart disease is far less established. Our previous work demonstrated that cardiomyocyte RASSF1A mediates apoptosis and promotes cardiac dysfunction and pathological remodeling in a pressure overload (PO)-induced model of heart failure (13). Cardiomyocyte-specific deletion of RASSF1A afforded protection against PO-induced failure, whereas cardiomyocyte-specific transgenic overexpression of RASSF1A exacerbated the heart failure phenotype in response to PO. Interestingly, systemic RASSF1A deletion resulted in augmented cardiac fibrosis and did not afford cardioprotection against PO-induced heart failure (13, 14). These results indicated cell type specificity of RASSF1A signaling that facilitated robust effects on cardiac remodeling and dysfunction. Our prior studies also indicated a role for RASSF1A in facilitating the activation of Mst1, and subsequent inhibition of Bcl-xL, to promote cardiomyocyte apoptosis (15). However, the function of RASSF1A in the heart during acute injury such as I/R has not been directly examined. Moreover, *in vivo* genetic manipulation to elucidate cell type–specific functions of RASSF1A in this cardiac injury model has not been reported.

The aim of this study was to investigate RASSF1A function during acute I/R injury in the heart. We utilized both systemic and cell type–specific knockout mice to demonstrate opposing effects of RASSF1A deletion in cardiomyocytes *versus* myeloid

This work was supported by National Institutes of Health Grants HL127339, HL122669, and HL135726 (to D. P. D.) and HL112330 (to J. S.) and the Leducq Fondation 15CBD04 (to J. S.). The authors declare that they have no conflicts of interest with the contents of this article. The content is solely the responsibility of the authors and does not necessarily represent the official views of the National Institutes of Health.

[1] Both authors contributed equally to this work.

[2] To whom correspondence should be addressed. Tel.: 973-972-1658; Fax: 973-972-8919; E-mail: delredo@njms.rutgers.edu.

[3] The abbreviations used are: MI, myocardial infarction; I/R, ischemia/reperfusion; BMDM, bone marrow–derived macrophage; α-MHC, α-myosin heavy chain; ANOVA, analysis of variance; ECM, extracellular matrix; TUNEL, terminal deoxynucleotidyltransferase-mediated dUTP nick-end labeling; AAR, area at risk; qPCR, quantitative PCR; TNFα, tumor necrosis factor α; IL, interleukin; LPS, lipopolysaccharide; LV, left ventricle; TTC, triphenyltetrazolium chloride; LVSd, LV end-systolic dimension; LVEF, left ventricular ejection fraction; PMSF, phenylmethylsulfonyl fluoride; LVDP, left ventricular developed pressure; PO, pressure overload; LVDd, LV end-diastolic dimension.

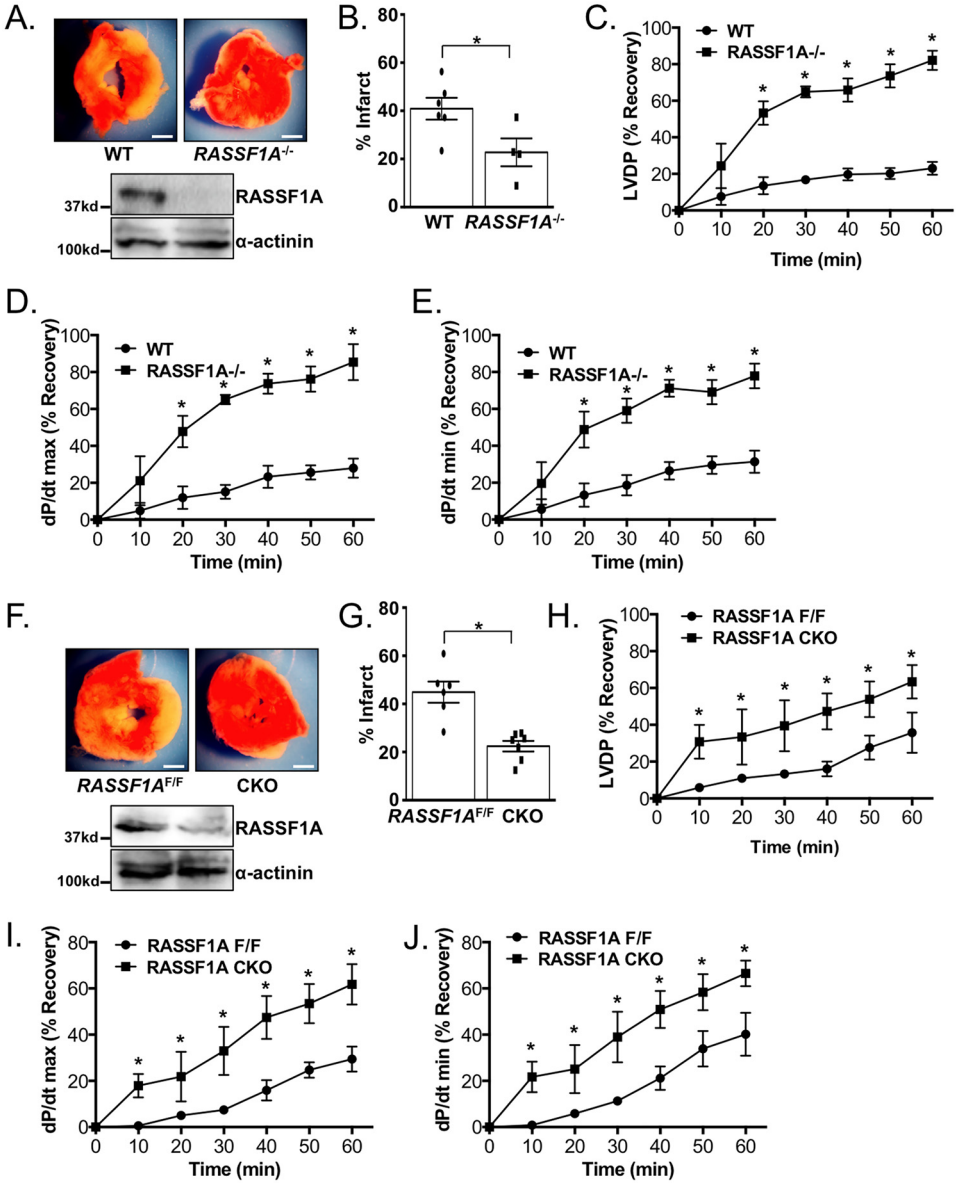

Figure 1. RASSF1A$^{-/-}$ and RASSF1A$^{F/F}$;αMHC-Cre (CKO) hearts are protected against global I/R *ex vivo* using a Langendorff preparation. *A* and *F*, representative images of TTC-stained heart sections (*upper panel*) and Western blottings (*lower panel*). *Scale bar*, 1 mm. *B* and *G*, percent infarct was determined using TTC staining. *C–E* and *H–J*, LVDP, d*P*/d*t* max, and d*P*/d*t* min were measured during the reperfusion phase using a pressure transducer and graphed as a percentage of baseline measurements (% recovery). *, $p < 0.05$. $n = 4–7$ mice/group.

cells on myocardial infarction. We report that RASSF1A negatively regulates the activity of NF-κB transcriptional output in macrophages. Our findings indicate that RASSF1A works to repress inflammatory cytokine expression in macrophages and propose RASSF1A to be an important endogenous "brake" to prevent excessive NF-κB activation and inflammatory cytokine production during I/R.

Results

Both systemic and cardiomyocyte-specific RASSF1A deletion are protective against global I/R injury

Our previous work demonstrated that cardiomyocyte-specific deletion of RASSF1A (RASSF1A$^{F/F}$;αMHC-Cre and referred to hereafter as RASSF1A CKO), but not systemic RASSF1A deletion (RASSF1A$^{-/-}$), attenuated cardiac hypertrophy, remodeling, and dysfunction in response to PO stress (13). Therefore, we sought to determine whether loss of RASSF1A in these genetic mouse models provided cardioprotection against I/R injury. We first used a Langendorff preparation to subject intact hearts to global I/R *ex vivo*, and we determined the extent of infarct by TTC staining and functional recovery using invasive hemodynamic measurement (16). We found that RASSF1A$^{-/-}$ hearts were significantly protected against global I/R, showing smaller infarcts and greater left ventricular developed pressure (LVDP) and d*P*/d*t* max and d*P*/d*t* min compared with wildtype (WT) littermate controls (Fig. 1, *A–E*). Cardiomyocyte-specific RASSF1A CKO mice were also subjected to global I/R and assessed. We found that RASSF1A CKO hearts had reduced infarcts and better heart function (LVDP, d*P*/d*t* max, and d*P*/d*t* min) compared with RASSF1A$^{F/F}$

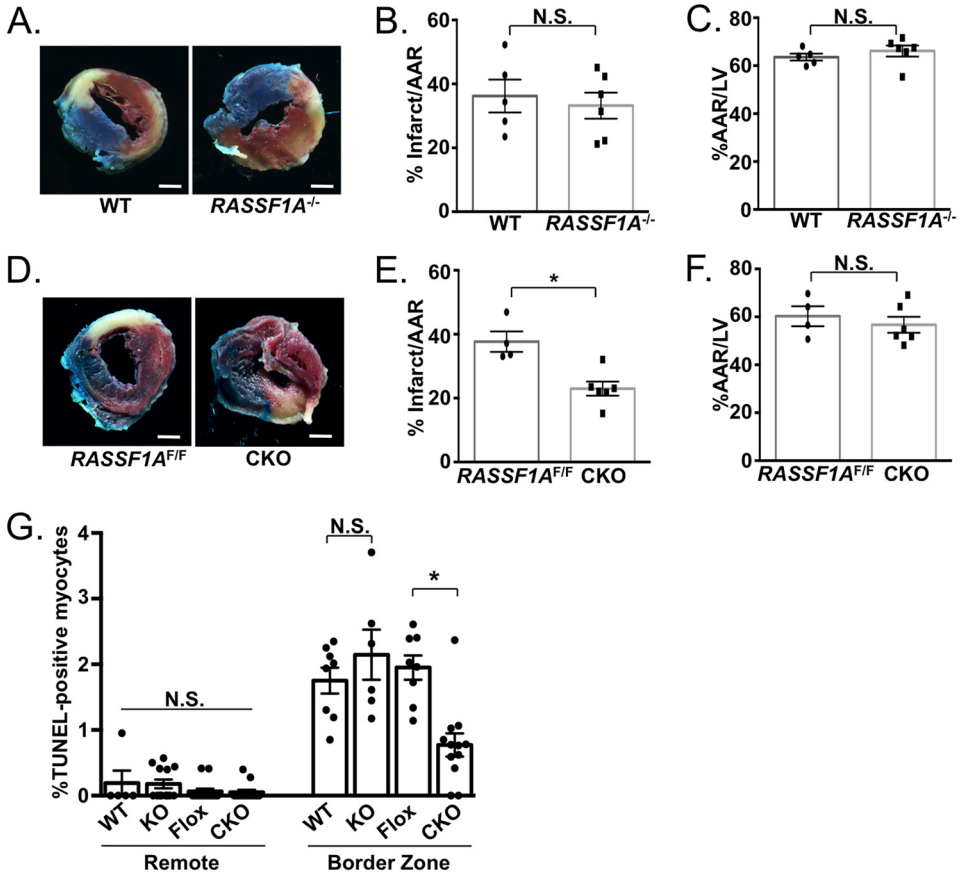

Figure 2. RASSF1A$^{-/-}$ mice do not exhibit cardioprotection against *in vivo* I/R. *A* and *D,* representative TTC/Alcian blue-stained heart sections. *B* and *C,* infarct size and AAR were similar between WT and RASSF1A$^{-/-}$ hearts. *E* and *F,* conversely, RASSF1A CKO mice had significantly smaller myocardial infarcts with no difference in AAR. *G,* extent of cardiomyocyte apoptosis was determined *in situ* by TUNEL and cardiac troponin T (*cTnT*) counterstaining. The percentage of TUNEL-positive cardiomyocyte nuclei was determined in the infarct border zone and the remote region. *Scale bar*, 1 mm. *G* (*Remote*), one-way ANOVA, F = 1.162, $p = 0.3363$; (*Border Zone*); one-way ANOVA, F = 8.742, $p < 0.001$. *, $p < 0.05$. *N.S.* = not significant. $n = 4–6$ mice/group.

controls, and the extent of cardioprotection was comparable with what was observed in RASSF1A$^{-/-}$ hearts (Fig. 1, *F–J*). Together, these results indicated that loss of RASSF1A function, either globally or restricted to cardiomyocytes, was sufficient to reduce injury caused by I/R in the isolated heart.

RASSF1A$^{-/-}$ hearts are not protected against in vivo I/R

To determine the role of RASSF1A in a model of I/R injury that is more relevant to MI patients, we subjected our mice to regional I/R by transiently occluding the left anterior descending artery *in vivo* (15). Surprisingly, we found that RASSF1A$^{-/-}$ mice were no longer afforded protection, as determined by no difference in infarct size between knockout and WT controls (Fig. 2, *A–C*). In contrast, the RASSF1A CKO mice had significantly smaller infarcts *versus* RASSF1A$^{F/F}$ controls in response to *in vivo* I/R (Fig. 2, *D–F*). Because myocyte loss drives infarct, we determined the extent of TUNEL-positive cardiomyocytes in the infarct border zone and remote regions after I/R. We observed no differences between groups in the remote region; however, there was a significant attenuation of apoptosis in RASSF1A CKO border zone myocytes compared with controls, whereas no difference was noted in RASSF1A systemic knockout mice (Fig. 2*G*). These results indicated that RASSF1A function in nonmyocytes plays an important role in modulating I/R injury, as well as cardiomyocyte apoptosis surrounding the infarct area. Additionally, based on our findings in isolated hearts, we reasoned the cellular source of this RASSF1A signal was likely extra-cardiac.

RASSF1A$^{-/-}$ hearts have augmented inflammation after injury

To better understand these phenotypic differences, we began to explore the potential role of RASSF1A in cardiac inflammation during I/R. Using the same mouse models as above, we performed additional *in vivo* I/R experiments and investigated the extent of inflammatory markers within the myocardium. Our results demonstrate that I/R increases the level of TNFα protein in WT myocardium compared with sham control (Fig. 3*A*). In the systemic RASSF1A$^{-/-}$ hearts, TNFα protein levels were further increased by I/R. In contrast, we did not observe any difference in TNFα protein between RASSF1A CKO and RASSF1A$^{F/F}$ control hearts, either in sham or I/R conditions (Fig. 3*B*). Staining of heart sections to detect the pan-macrophage marker F4/80 demonstrated similar results (Fig. 3*C*). We also performed immunostaining for TNFα and observed a significant increase in TNFα-positive nonmyocytes in RASSF1A$^{-/-}$ hearts after I/R compared with WT (Fig. 3, *D* and *E*), whereas the number of TNFα-positive nonmyocytes in RASSF1A CKO hearts was significantly attenuated compared with controls (Fig. 3, *F* and *G*). Additionally, we coun-

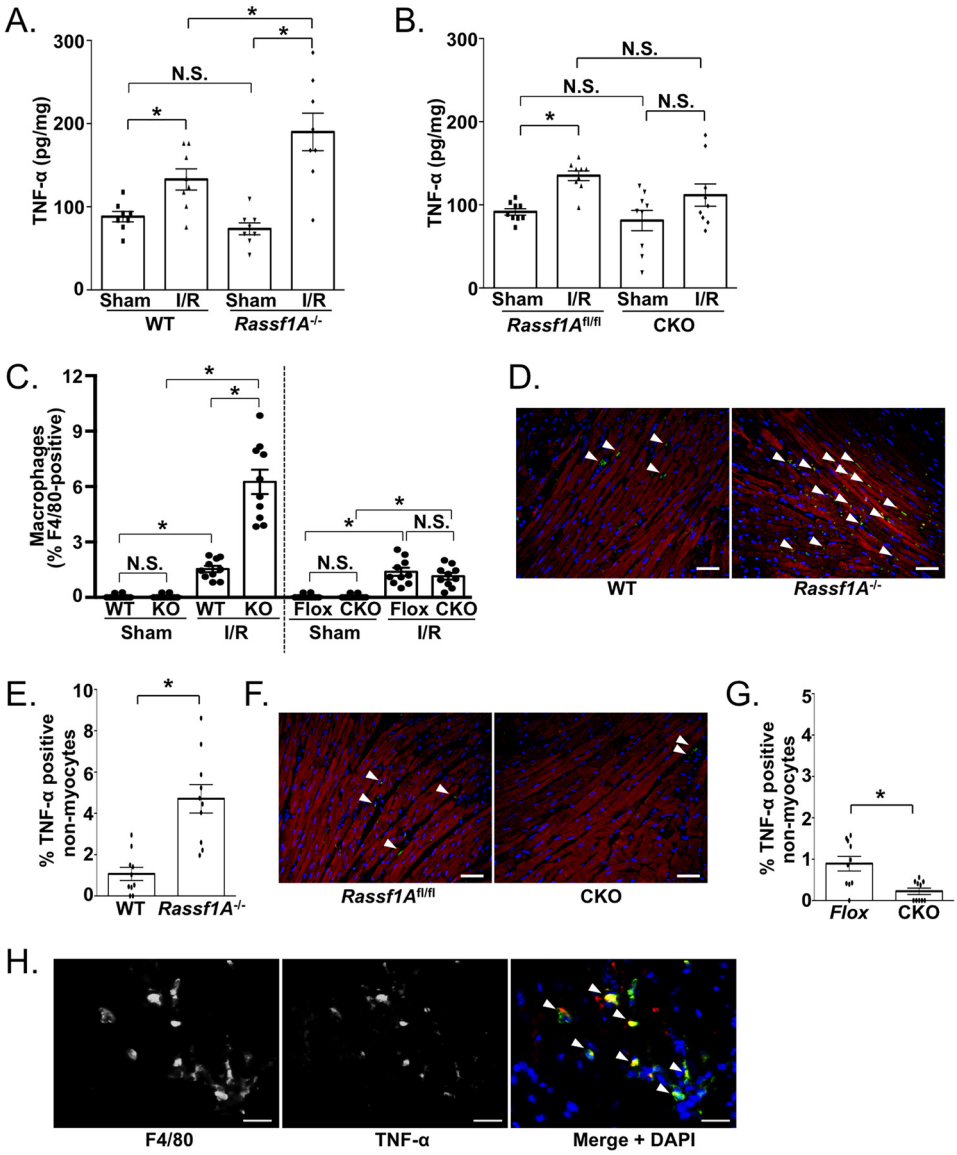

Figure 3. Enhanced cardiac inflammation in RASSF1A$^{-/-}$ mice after I/R. Following I/R (30 min/24 h), the levels of TNFα protein (*A* and *B*), F4/80-positive macrophages (*C*), and TNFα-positive nonmyocytes (*D–G*) were significantly increased in RASSF1A$^{-/-}$ (KO) hearts but not in RASSF1A CKO hearts compared with respective controls. *H,* immunostaining revealed co-localization of macrophages (F4/80) and TNFα-positive cells (*arrows*) in the infarct border zone following I/R (30 min/24 h) in C57BL/6 WT mice. *Scale bar*, 30 μm. *A*, two-way ANOVA: genotype, F = 2.340, $p = 0.137$. Treatment, F = 34.080, $p < 0.001$. Genotype × treatment, F = 6.724, $p = 0.015$. *B*, two-way ANOVA: genotype, F = 2.998, $p = 0.093$. Treatment, F = 14.476, $p = 0.001$. Genotype × treatment, F = 0.444, $p = 0.510$. *C*, two-way ANOVA: genotype, F = 47.646, $p < 0.001$. Treatment, F = 126.331, $p < 0.001$. Genotype × treatment, F = 47.548, $p < 0.001$. *, $p < 0.05$. *N.S.* = not significant. $n = 4–6$ mice/group.

terstained WT heart sections to detect TNFα and F4/80 and observed prominent signal overlap, suggesting that macrophages are a major source of cardiac TNFα in response to I/R (Fig. 3*H*). These findings indicated that loss of RASSF1A in nonmyocytes exaggerated inflammation caused by I/R in the heart.

Myeloid deletion of RASSF1A increases I/R injury

Previous work has demonstrated that shortly after ischemic insult, bone marrow and splenic monocytes are recruited to and infiltrate the myocardium, where they differentiate to macrophages and participate in the injury response (17, 18). Myeloid cells recruited during this initial phase exhibit a pro-inflammatory phenotype and express high levels of cytokines, including TNFα, IL-1β, and IL-6. The function of RASSF1A in the myeloid compartment, and its potential contribution to I/R inflammation and injury, is not known. Therefore, we selectively targeted RASSF1A for deletion in these cells using LysM-Cre transgenic mice (19). Baseline analysis did not reveal any obvious abnormalities in the heart, lung, or spleen in RASSF1A$^{F/F}$;LysM-Cre mice. Cardiac systolic function and dimensions, as well as immune cell composition, also showed no difference between RASSF1A$^{F/F}$;LysM-Cre and RASSF1A$^{F/F}$ control mice (Table 1). However, following I/R, we observed augmented infarct size in RASSF1A$^{F/F}$;LysM-Cre hearts compared with controls (Fig. 4, *A–C*). Serum levels of cardiac troponin I were also significantly increased in RASSF1A$^{F/F}$;LysM-Cre mice compared with control mice after I/R (Fig. 4*D*). Taken together,

Table 1
Baseline characterization of control and RASSF1A;LysM-Cre mice
Data are presented as mean ± S.E.M. The following abbreviations are used: Left ventricle weight/tibia length (LV/TL), LVEF, LVDd, diastolic septal wall thickness (SWT), and diastolic posterior wall thickness (PWT).

Parameter	RASSF1A$^{F/F}$	RASSF1A$^{F/F}$;LysM-Cre
n	3	4
LV/TL (mg/mm)	5.31 ± 0.38	5.51 ± 0.28
Lung/TL (mg/mm)	7.22 ± 0.19	7.39 ± 0.31
Spleen/TL (mg/mm)	9.03 ± 0.60	8.62 ± 0.83
LVEF (%)	79.3 ± 1.5	81.3 ± 0.6
LVDd (mm)	3.57 ± 0.14	3.32 ± 0.07
SWT (mm)	0.77 ± 0.03	0.79 ± 0.02
PWT (mm)	0.74 ± 0.03	0.76 ± 0.03
% of blood CD45+		
Monocyte	3.29 ± 0.09	2.24 ± 0.49
Neutrophil	10.84 ± 2.56	11.09 ± 0.80
T cell	18.57 ± 0.09	21.43 ± 1.14
B cell	38.03 ± 3.33	35.36 ± 1.48

these results indicate enhanced cardiac injury in RASSF1A$^{F/F}$;LysM-Cre mice.

Myeloid deletion of RASSF1A increases cardiac inflammation after I/R

To determine whether RASSF1A$^{F/F}$;LysM-Cre mice had an augmented cardiac inflammatory response following *in vivo* I/R, we performed qPCR to detect mRNA expression of pro-inflammatory genes from infarcted tissue. Our results demonstrated increased cardiac expression of *TNFα*, *IL-1β*, *Nos2*, and *Cox2* in both RASSF1A$^{F/F}$ control mice and RASSF1A$^{F/F}$;LysM-Cre mice after I/R. However, expression levels of each gene were increased to a greater extent in RASSF1A$^{F/F}$;LysM-Cre compared with control hearts, indicating an enhanced immune response to injury (Fig. 4, *E–H*). Additionally, we detected macrophages using immunofluorescence and found that RASSF1A$^{F/F}$;LysM-Cre hearts had higher numbers of F4/80-positive cells compared with RASSF1A$^{F/F}$ controls in response to I/R (Fig. 4, *I* and *J*). Together, our data demonstrate a more robust inflammatory response to heart injury in RASSF1A$^{F/F}$;LysM-Cre mice.

Cardiac remodeling–associated gene expression is altered in RASSF1A mutant mice

Cardiac inflammation and inflammatory cell infiltration are important modulators of fibrosis, scar formation, and remodeling of the heart after injury. To determine whether these processes may also be altered in the RASSF1A mutant mice, we examined gene expression of established regulators of fibrosis and extracellular matrix (ECM) remodeling. Following 24 h of reperfusion, we isolated and compared infarcted tissue with myocardium from sham-operated control mice. We found that in cardiomyocyte-deficient RASSF1A hearts, expression of most of the genes analyzed was significantly lower compared with control mice, both in sham and I/R conditions (Fig. 5, *A–F*). Conversely, we observed that expression of most of these genes was significantly greater in myeloid-deficient RASSF1A hearts after I/R, but not at baseline (sham) conditions (Fig. 5, *G–L*). This opposite cell type–specific effect of RASSF1A targeting is in agreement with our injury and inflammation results and suggests that myeloid deletion of RASSF1A may also exacerbate fibrosis and remodeling of the heart following I/R injury.

RASSF1A represses NF-κB activity in macrophages

Next, we questioned whether RASSF1A functionally interacts with NF-κB, a master regulator of inflammatory gene expression, using RAW264.7 mouse macrophages. To test this hypothesis, we performed both RASSF1A gain- and loss–of–function experiments. We found that RASSF1A overexpression was sufficient to significantly attenuate both baseline and TNFα-induced NF-κB luciferase activity (Fig. 6, *A* and *B*). Conversely, we found that siRNA-mediated knockdown of RASSF1A was sufficient to increase NF-κB activation (Fig. 6, *C* and *D*). In response to RASSF1A knockdown, we also observed increased mRNA expression of *IL-1β*, *TNFα*, *Nos2*, and *Cox2*, established transcriptional targets of NF-κB, whereas no changes in genes associated with the resolution of inflammation were altered by RASSF1A depletion (Fig. 6, *E* and *F*). To enhance the relevance of our findings, we isolated and cultured bone marrow–derived macrophages (BMDMs) from control and RASSF1A$^{F/F}$;LysM-Cre mice. In BMDMs deficient for RASSF1A, we observed significantly higher expression of *IL-1β*, *TNFα*, *Nos2*, and *Cox2* mRNA following TNFα challenge. However, expression of these genes was comparable between RASSF1A$^{F/F}$;LysM-Cre BMDMs and control cells at baseline (Fig. 6, *G–K*). Importantly, we also found enhanced protein expression of IL-1β in LPS-treated RASSF1A$^{F/F}$;LysM-Cre BMDMs (Fig. 6*L*). Together, these data indicate that RASSF1A negatively regulates macrophage NF-κB activity and target gene expression in a cell-autonomous manner.

RASSF1A negatively regulates YAP to restrain NF-κB in macrophages

Our previous work demonstrated that RASSF1A promotes apoptosis through the activation of Mst1 and stimulation of noncanonical Hippo signaling in the cardiomyocyte (13, 15). To investigate whether RASSF1A engages Mst1 and the Hippo pathway in the macrophage, we either overexpressed or knocked down RASSF1A in RAW264.7 cells. Increased RASSF1A expression caused Mst1 activation and the down-regulation of YAP protein levels (Fig. 7*A*). Conversely, siRNA-mediated silencing of RASSF1A increased the presence of nuclear YAP and up-regulated the mRNA levels of established YAP target genes, *Cyr61* and *Ctgf* (Fig. 7, *B–D*). To determine whether YAP mediated the enhanced inflammatory gene expression elicited by RASSF1A silencing, we simultaneously knocked down RASSF1A and YAP in macrophages. Our results indicated that cytokine mRNA levels were normalized following depletion of both RASSF1A and YAP (Fig. 7, *E–G*), implicating Hippo signaling in this response. To further elucidate how YAP modulates NF-κB, we performed co-immunoprecipitation experiments against FLAG–YAP or endogenous RelA, the p65 subunit of NF-κB, in RAW264.7 cells. Our results demonstrate association between YAP and RelA (Fig. 7*H*). We next examined whether YAP localized to κB-binding elements within the promoters of two established NF-κB target genes. Indeed, we were able to detect exogenously expressed YAP at the promoters of *TNFα* and *IL-1β* as determined by ChIP assay (Fig. 7, *I* and *J*). Together, these results indicate that YAP can bind to RelA and is present on DNA at NF-κB recognition sites.

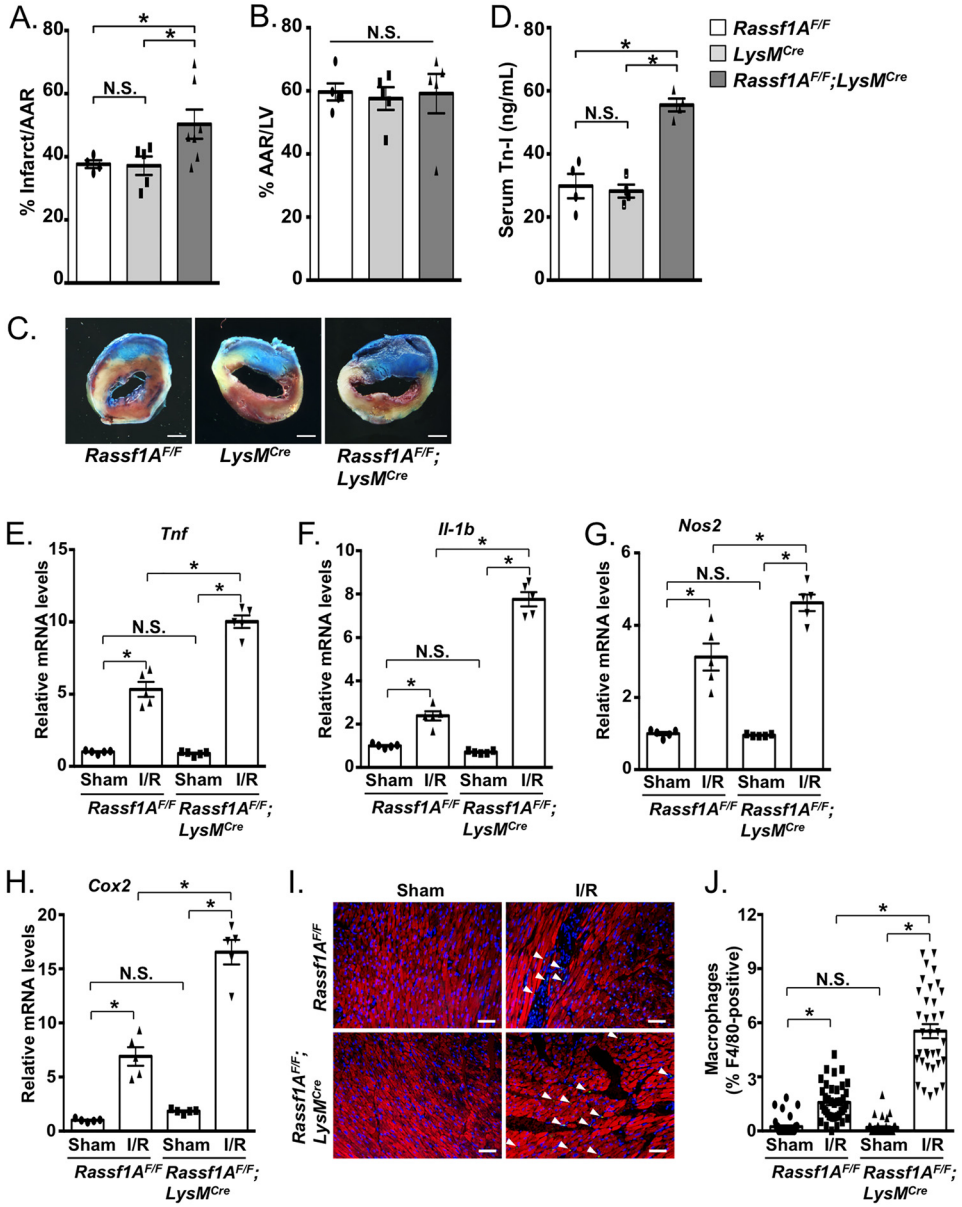

Figure 4. Myeloid RASSF1A restrains inflammation and attenuates heart injury. *A–C*, myeloid-specific deletion of RASSF1A (RASSF1A$^{F/F}$;LysM-Cre) increased infarct size after I/R (30 min/24 h) with no difference in AAR compared with controls. *Scale bar*, 1 mm. *D*, myeloid-specific deletion of RASSF1A increased serum cardiac troponin-I levels following I/R (30 min/24 h) compared with control mice. *E–H*, RASSF1A$^{F/F}$;LysM-Cre and RASSF1A$^{F/F}$ control mice were subjected to I/R (30 min/24 h) or sham operation. Following RNA isolation from infarcted tissue, qPCR was performed to determine expression of inflammatory genes. *I* and *J*, immunostaining revealed enhanced presence of F4/80-positive cells in RASSF1A$^{F/F}$;LysM-Cre hearts compared with RASSF1A$^{F/F}$ control hearts following I/R (30 min/24 h). *Scale bar*, 30 μm. *A*, one-way ANOVA, F = 3.908, $p = 0.0469$. *B*, one-way ANOVA, F = 0.05981, $p = 0.9422$. *D*, one-way ANOVA, F = 29.88, $p < 0.001$. *E*, two-way ANOVA: genotype, F = 46.587, $p < 0.001$. Treatment, F = 402.926, $p < 0.001$. Genotype × treatment, F = 50.875, $p < 0.001$. *F*, two-way ANOVA: genotype, F = 166.0880, $p < 0.001$. Treatment, F = 456.643, $p < 0.001$. Genotype × treatment, F = 205.969, $p < 0.001$. *G*, two-way ANOVA: genotype, F = 10.724, $p = 0.005$. Treatment, F = 171.749, $p < 0.001$. Genotype × treatment, F = 12.201, $p = 0.003$. *H*, two-way ANOVA: genotype, F = 54.034, $p < 0.001$. Treatment, F = 209.152, $p < 0.001$. Genotype × treatment, F = 38.140, $p < 0.001$. *J*, two-way ANOVA: genotype, F = 94.965, $p < 0.001$. Treatment, F = 276.116, $p < 0.001$. Genotype × treatment, F = 98.679, $p < 0.001$. *, $p < 0.05$. *N.S.*, not significant. $n = 5–13$ mice/group.

Discussion

Many chronic pathologies, including cardiovascular disease and stroke, metabolic disease and diabetes, autoimmune diseases, and cancers, have heightened inflammatory states that are thought to contribute to disease progression. Therefore, the identification of novel regulatory mechanisms to modulate inflammation may lead to more effective therapeutic options for patients. Prior work has implicated RASSF1A as a negative regulator of inflammation using a mouse model of chemically-induced colitis (20). A separate study demonstrated enhanced immune cell infiltration in RAS-driven lung tumors in mice with global RASSF1A deficiency (21). Importantly, however, whether loss of RASSF1A function modulates cardiac inflammation and injury caused by I/R had not been investigated. Moreover, the important cell type(s) *in vivo* that mediate the effect of RASSF1A on inflammation remained to be elucidated. The results of our study demonstrate that loss of RASSF1A function selectively within myeloid cells caused increased

inflammation and injury of the myocardium resulting from I/R. This is in contrast to cardiomyocyte-specific RASSF1A deletion, which affords reduced infarct triggered by I/R. Using primary BMDMs and RAW264.7 cells, we demonstrated that modulation of RASSF1A causes altered activation status of NF-κB and subsequent pro-inflammatory cytokine expression. Additionally, we observed that RASSF1A engages the Hippo pathway to activate Mst1 and inhibit YAP function and that concomitant RASSF1A and YAP knockdown largely normalized the inflammatory gene expression in macrophages. We also report that YAP associates with RelA and is present on κB elements in NF-κB target genes. These results provide further evidence that RASSF1A acts as a

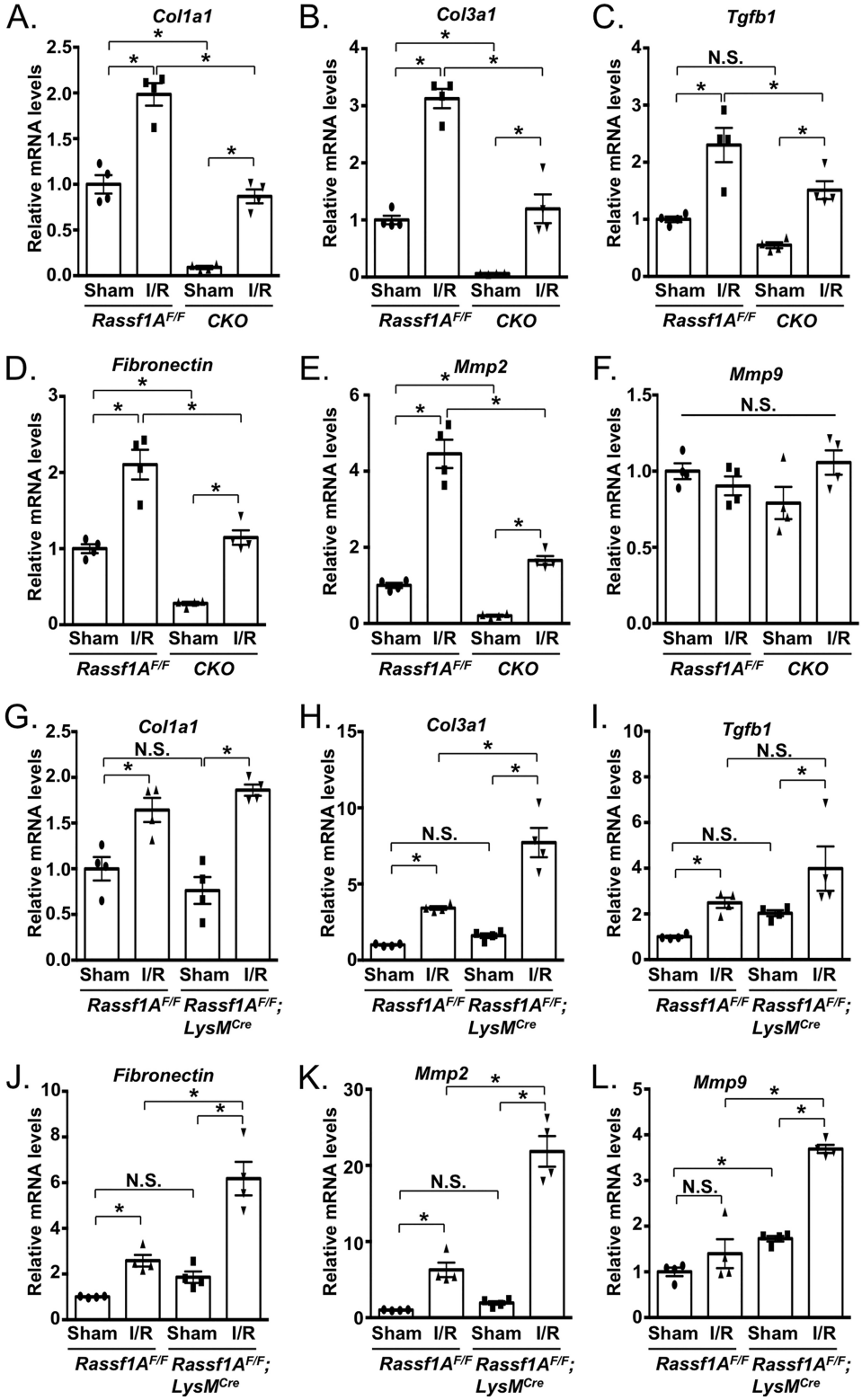

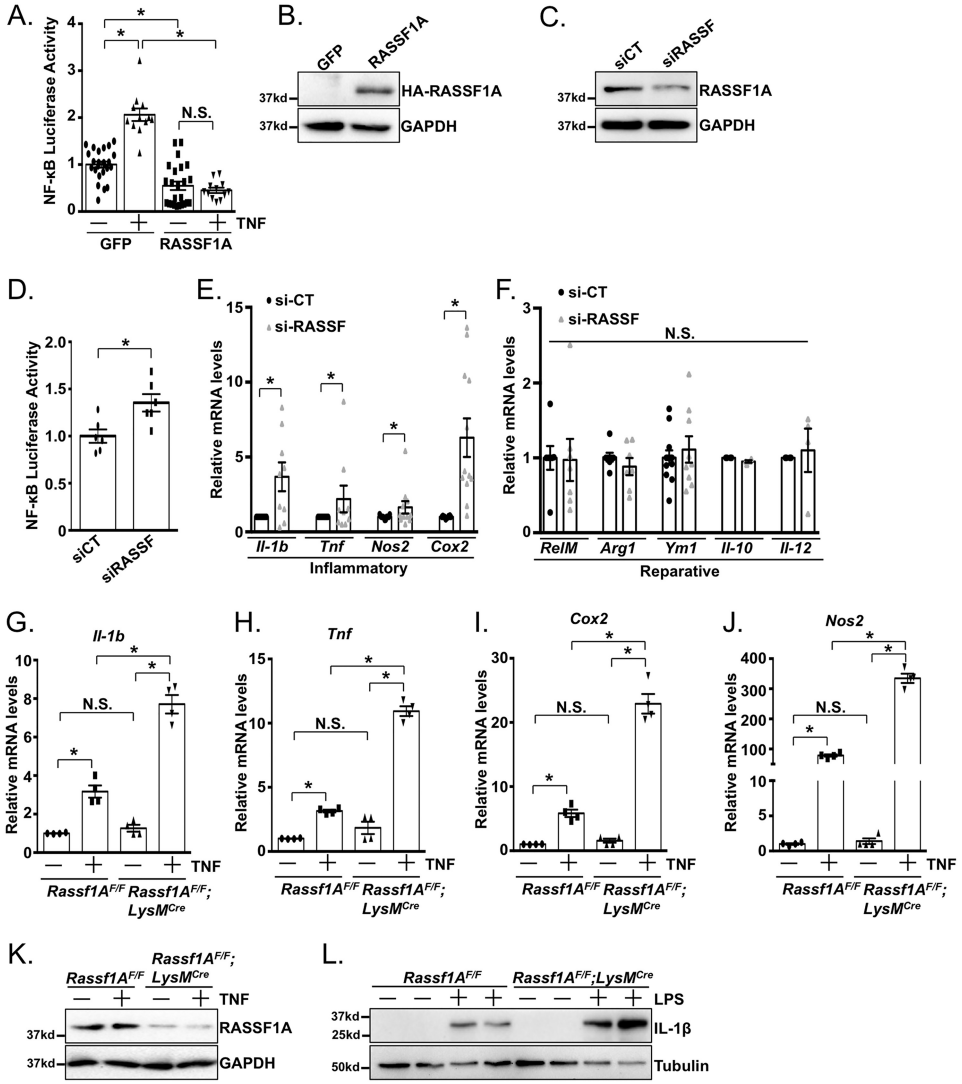

Figure 6. RASSF1A negatively regulates NF-κB in macrophages. *A* and *B,* increased RASSF1A expression inhibited basal and TNFα-induced NF-κB transcriptional activation as determined by luciferase reporter assay in RAW264.7 cells. *C–F*, knockdown of RASSF1A increased NF-κB luciferase reporter activation and pro-inflammatory cytokine expression, with no effect on genes associated with wound healing. *G–K,* isolation and TNFα stimulation of BMDMs from RASSF1A$^{F/F}$ control and RASSF1A$^{F/F}$;LysM-Cre mice revealed augmented *TNFα*, *IL-1β*, *Nos2*, and *Cox2* mRNA expression in RASSF1A$^{F/F}$;LysM-Cre cells following TNFα stimulation. *L*, Western blotting demonstrating increased IL-1β protein in LPS-stimulated RASSF1A$^{F/F}$;LysM-Cre BMDMs. *A*, two-way ANOVA: plasmid, F = 118.856, $p < 0.001$. Treatment, F = 25.946, $p < 0.001$. Plasmid × treatment, F = 37.628, $p < 0.001$. *G*, two-way ANOVA: genotype, F = 63.476, $p < 0.001$. Treatment, F = 204.243, $p < 0.001$. Genotype × treatment, F = 50.173, $p < 0.001$. *H*, two-way ANOVA: genotype, F = 191.229, $p < 0.001$. Treatment, F = 324.964, $p < 0.001$. Genotype × treatment, F = 123.830, $p < 0.001$. *I*, two-way ANOVA: genotype, F = 259.883, $p < 0.001$. Treatment, F = 666.224, $p < 0.001$. Genotype × treatment, F = 258.266, $p < 0.001$. *J*, two-way ANOVA: genotype, F = 112.996, $p < 0.001$. Treatment, F = 248.670, $p < 0.001$. Genotype × treatment, F = 98.893, $p < 0.001$. *, $p < 0.05$. *N.S.* = not significant. n = 3–4 experimental replicates.

negative regulator of inflammation, implicates Hippo–YAP signaling as a mediator of this response, and demonstrates the pathological importance of this mechanism for I/R injury.

NF-κB is a central regulator of innate immune responses and stimulates expression of numerous pro-inflammatory cytokines to promote inflammation (22). In this study, we identify

Figure 5. Cell type–specific effect of RASSF1A on ECM-related gene expression. *A–F,* RASSF1A$^{F/F}$;αMHC-Cre and control mice were subjected to sham or I/R (30 min/24 h). RNA was isolated from infarcted tissue or control myocardium, and qPCR was performed. *G–L,* RASSF1A$^{F/F}$;LysM-Cre and control mice were subjected to sham or I/R (30 min/24 h). RNA was isolated from infarcted tissue or control myocardium, and qPCR was performed. *A*, two-way ANOVA: genotype, F = 175.316, $p < 0.001$. Treatment, F = 144.076, $p < 0.001$. Genotype × treatment, F = 2.659, $p = 0.129$. *B*, two-way ANOVA: genotype, F = 85.004, $p < 0.001$. Treatment, F = 109.842, $p < 0.001$. Genotype × treatment, F = 10.181, $p = 0.008$. *C*, two-way ANOVA: genotype, F = 13.027, $p = 0.004$. Treatment, F = 43.303, $p < 0.001$. Genotype × treatment, F = 0.956, $p = 0.348$. *D*, two-way ANOVA: genotype, F = 55.716, $p < 0.001$. Treatment, F = 76.727, $p < 0.001$. Genotype × treatment, F = 1.128, $p = 0.309$. *E*, two-way ANOVA: genotype, F = 81.941, $p < 0.001$. Treatment, F = 153.061, $p < 0.001$. Genotype × treatment, F = 25.413, $p < 0.001$. **F**, two-way ANOVA: genotype, F = 0.130, $p = 0.725$. Treatment, F = 1.194, $p = 0.296$. Genotype × treatment, F = 5.445, $p = 0.038$. *G*, two-way ANOVA: genotype, F = 0.007, $p = 0.936$. Treatment, F = 51.445, $p < 0.001$. Genotype × treatment, F = 3.524, $p = 0.085$. *H*, two-way ANOVA: genotype, F = 24.775, $p < 0.001$. Treatment, F = 75.036, $p < 0.001$. Genotype × treatment, F = 14.032, $p = 0.003$. *I*, two-way ANOVA: genotype, F = 6.314, $p = 0.027$. Treatment, F = 11.654, $p = 0.005$. Genotype × treatment, F = 0.213, $p = 0.653$. *J*, two-way ANOVA: genotype, F = 29.861, $p < 0.001$. Treatment, F = 52.441, $p < 0.001$. Genotype × treatment, F = 11.208, $p = 0.006$. *K*, two-way ANOVA: genotype, F = 54.189, $p < 0.001$. Treatment, F = 126.231, $p < 0.001$. Genotype × treatment, F = 42.513, $p < 0.001$. *L*, two-way ANOVA: genotype, F = 75.747, $p < 0.001$. Treatment, F = 46.239, $p < 0.001$. Genotype × treatment, F = 20.408, $p = 0.001$. *, $p < 0.05$. *N.S.* = not significant. n = 4 mice/group.

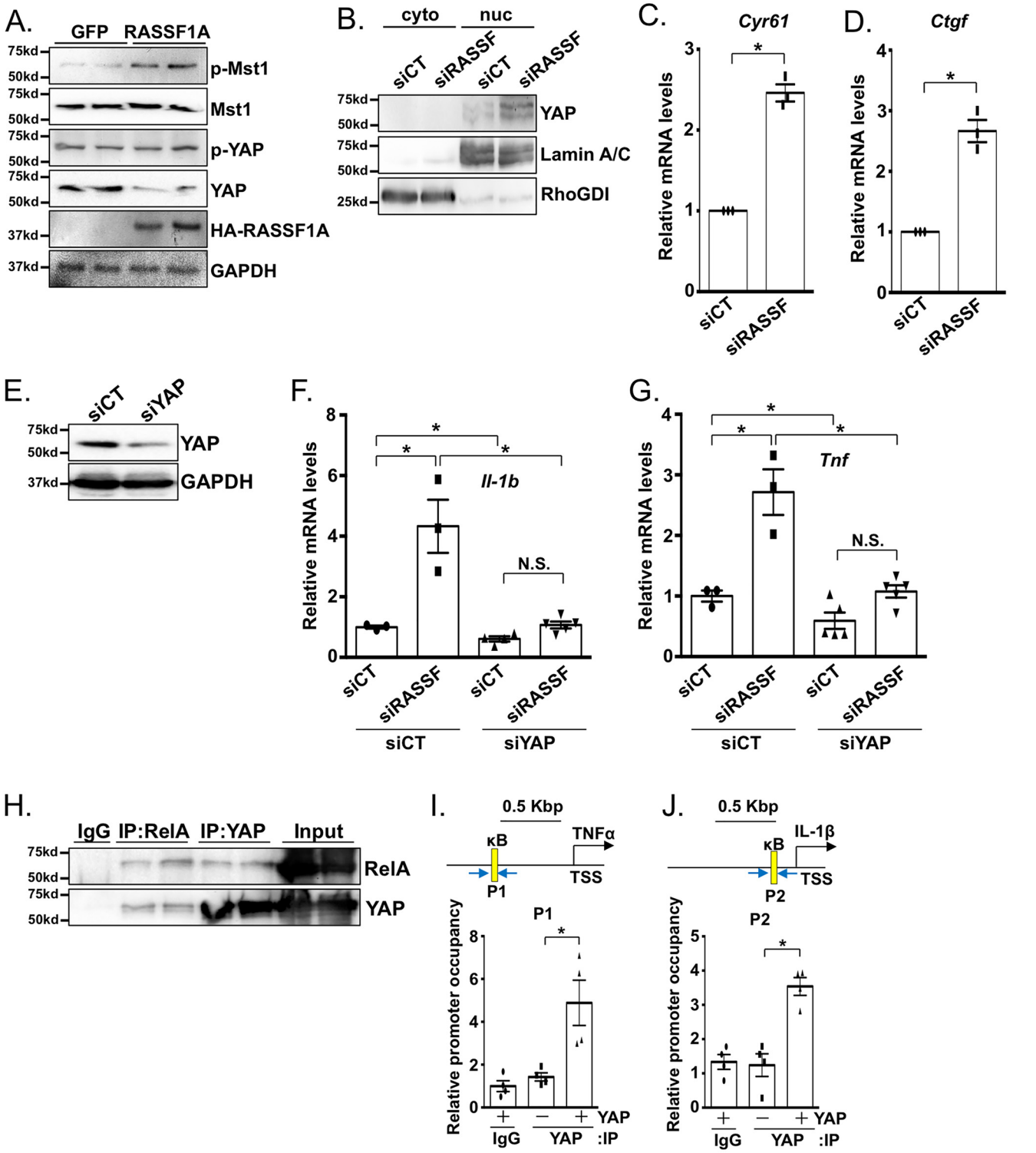

Figure 7. RASSF1A inhibits YAP in macrophages. *A,* RASSF1A activated Mst1 signaling and inhibited YAP in RAW264.7 macrophages. *B–D,* knockdown of endogenous RASSF1A increased nuclear accumulation of YAP and increased mRNA expression of YAP target genes, *Cyr61* and *Ctgf*. *E–G,* concomitant knockdown of RASSF1A and YAP abrogated the up-regulation of inflammatory cytokines caused by RASSF1A silencing alone. *H,* co-immunoprecipitation of FLAG–YAP or endogenous RelA demonstrated association in RAW264.7 cells. *I* and *J,* ChIP assays demonstrated YAP presence at κB elements in promoters of *TNFα* and *IL-1β* genes in RAW264.7 cells. *F*, two-way ANOVA: RASSF1A, $F = 28.565$, $p < 0.001$. YAP, $F = 26.544$, $p < 0.001$. RASSF1A × YAP, $F = 16.361$, $p = 0.002$. *G*, two-way ANOVA: RASSF1A, $F = 36.735$, $p < 0.001$. YAP, $F = 31.822$, $p < 0.001$. RASSF1A × YAP, $F = 11.531$, $p = 0.005$. *I*, one-way ANOVA, $F = 11.22$, $p = 0.0036$. *J*, one-way ANOVA, $F = 22.47$, $p < 0.001$. *, $p < 0.05$. $n = 3–4$ experimental replicates.

RASSF1A as a modulator of NF-κB activity in the macrophage. Specifically, we provide evidence that depletion of endogenous RASSF1A, either through siRNA-mediated silencing in RAW264.7 cells or by Cre-mediated gene deletion in the myeloid compartment *in vivo*, promotes NF-κB activation and target gene expression. Interestingly, we observed acute up-regulation of

pro-inflammatory cytokines in response to RASSF1A knockdown, but we saw no change in genes associated with the reparative macrophage phenotype. Whereas a link between RASSF1A and inflammation has been reported previously (20, 21), our study is the first to investigate this mechanism through genetic targeting of RASSF1A in myeloid cells *in vivo*, and it is the first to demonstrate an associated pathophysiological effect in the myocardium during I/R injury.

There is a growing literature describing the different resident cardiac macrophage subtypes, as well as recruited monocyte subtypes, and their relative contribution to heart injury and the progression of heart disease (17, 23–29). Our approach is limited in that we used the LysM-Cre driver line to deplete RASSF1A globally in the myeloid compartment (19). This alone does not allow for delineating the relative contribution of resident *versus* recruited macrophage subtypes. However, as our understanding of these specific cell subtypes advances, as well as our ability to manipulate them (29, 30), future experiments may allow us to examine RASSF1A function in cardiac macrophage subsets and determine potential varied effects on inflammation and infarct.

Our results indicate that RASSF1A is an important negative regulator of inflammation and functions to suppress cytokine production following cardiac injury *in vivo*, and suggest that RASSF1A may be a potential therapeutic target for treatment of inflammatory conditions. This RASSF1A-mediated regulatory mechanism could have broad implications not only for MI and heart disease but may also be applicable to aberrant inflammatory pathologies in general.

Experimental procedures

Animal models

RASSF1A$^{-/-}$ and RASSF1A floxed mutant mice were a kind gift from Dr. Louise van der Weyden (31). The cardiomyocyte (αMHC) and myeloid (LysM) Cre recombinase transgenic mice have been described previously (19, 32). Male mice, aged 8–12 weeks, weighing 20–25 g were housed in a temperature-controlled environment with 12-h light/dark cycles where they received food and water *ad libitum*. All protocols concerning the use of animals were approved by the Institutional Animal Care and Use Committee, New Jersey Medical School, Rutgers University.

Myocardial ischemia/reperfusion

Prior to anesthesia, cephazolin (60 mg/kg) was administered (intraperitoneal injection) to prevent infection. Mice were anesthetized by intraperitoneal injection of pentobarbital sodium (50 mg/kg). Once anesthetized, mice were intubated and ventilated with a tidal volume of 0.2 ml and a respiratory rate of 110 breaths/min using 65% oxygen (rodent ventilator model 683; Harvard Apparatus Inc.). The animals were kept warm with heat lamps. Rectal temperature was monitored and maintained between 36 and 37 °C. The heart was exposed by a thoracotomy through the 4th and 5th ribs. The left coronary artery was located, and a suture was passed under the artery. To occlude the artery, a short length of tubing was threaded through the suture ends, and occlusion was effected by placing tension on the suture such that the tube compressed the artery. Ischemia was confirmed by ECG change (ST segment elevation). After occlusion for 30 min, the silicon tubing was removed to achieve reperfusion, and the rib space and overlying muscles were closed in layers using 5.0 nylon sutures. For sham operation, the same protocol was followed; however, no ligation of the coronary artery was performed. Postoperatively, mice were administered Buprenex-SR (1.2 mg/kg) subcutaneously for analgesia. Mice were then allowed to recover under close monitoring in an incubator. During this time, mice were observed for signs of post-operative complications, including pain, pneumothorax, and acute heart failure or sudden death (15).

Measurement of infarct size

Twenty four hours after reperfusion, mice were anesthetized and intubated, and the chest was opened. After the heart was arrested at the diastolic phase by KCl injection, the ascending aorta was cannulated and perfused with saline to wash out blood. The left anterior descending coronary artery was occluded with the same suture, which had been left at the site of the ligation. To demarcate the ischemic area at risk (AAR), Alcian blue dye (1%) was perfused into the aorta and coronary arteries. Hearts were excised, and LVs were sliced into 1-mm–thick cross-sections and incubated with a 1% TTC solution at 37 °C for 15 min. The infarct area (pale), the AAR (not blue), and the total LV area from both sides of each section were measured with the use of Adobe Photoshop (Adobe Systems Inc.), and the values obtained were averaged. The percentages of area of infarction and AAR of each section were multiplied by the weight of the section and then totaled from all sections. AAR/LV and infarct area/AAR were expressed as percentages (33).

Langendorff perfusion model

Mice were anesthetized with pentobarbital (65 mg/kg, i.p.) and treated intraperitoneally with 50 units of heparin. The heart was quickly removed and catheterized with a 22-gauge needle. The hearts were mounted on a Langendorff-type isolated heart perfusion system and subjected to retrograde coronary artery reperfusion with 37 °C oxygenated Krebs-Henseleit bicarbonate buffer (NaCl 120 mmol/liter, glucose 17 mmol/liter, $NaHCO_3$ 25 mmol/liter, KCl 5.9 mmol/liter, $MgCl_2$ 1.2 mmol/liter, $CaCl_2$ 2.5 mmol/liter, EDTA 0.5 mmol/liter) (pH 7.4), at a constant pressure of 80 mm Hg. A balloon filled with water was introduced into the left ventricle (LV) through the mitral valve orifice and connected to a pressure transducer via a plastic tube primed with water. LV pressures and LV dP/dt were recorded with a strip chart recorder (Astro-Med, Inc.). The LV end-diastolic pressure was set at 4–10 mm Hg at the beginning of perfusion by adjusting the volume of the balloon in the LV, and the volume was kept constant throughout an experiment. After a 30-min equilibration period, the heart was subjected to 30 min of global ischemia (at 37 °C) followed by 60 min of reperfusion.

Echocardiography

Mice were anesthetized using 12 μl/g body weight of 2.5% tribromoethanol (Avertin, Sigma), and echocardiography was

performed, as described previously (34), using a 13-MHz linear ultrasound transducer. Two-dimensional guided M-mode measurements of LV internal diameter were obtained from at least three beats and then averaged. LV end-diastolic dimension (LVDd) was measured at the time of the apparent maximal LV diastolic dimension, and LV end-systolic dimension (LVSd) was measured at the time of the most anterior systolic excursion of the posterior wall. LVEF was calculated using the following formula: LVEF (%) = $100 \times (LVDd^3 - LVSd^3)/LVDd^3$.

Cell culture and reagents

The RAW264.7 cell line was purchased from ATCC (TIB-71) and maintained according to established protocols (35). For BMDM experiments, bone marrow cells were isolated from adult RASSF1A$^{F/F}$;LysM-Cre and control RASSF1A$^{F/F}$ mice (36). Cells were cultured in complete RPMI 1640 medium supplemented with 10 ng/ml recombinant M-CSF (PeproTech) for 8–9 days. Cells were serum-starved 24 h prior to stimulation. Mouse recombinant TNFα was purchased from R&D Systems. LPS was purchased from Sigma.

Flow cytometry

Peripheral blood was collected from mice by retro-orbital bleeding. Red blood cells were lysed (BioLegend), and single cell suspensions were stained in 0.1% BSA/PBS buffer for 30 min at 4 °C using the following primary antibodies: anti-CD45 (clone 30-F11, BioLegend), anti-Ly6C (clone 1G7.G10, Miltenyi), anti-Ly6G (clone 1A8, BioLegend), anti-CD11b (clone M1/70, BioLegend), anti-CD3 (clone 17A2, eBioscience), and anti-CD19 (clone 1D3, eBioscience). Cells were washed and then fixed in 1% paraformaldehyde. An LSRForessa X-20 (BD Biosciences) was used to collect events, and analysis was performed using FlowJo software (Tree Star).

Expression constructs and siRNA

pCMV5-HA-RASSF1A was a gift from Joseph Avruch (Addgene plasmid no. 1980) (37). pCMV-FLAG-S127A-YAP was a gift from Kunliang Guan (Addgene plasmid no. 27370) (38). siRNA-mediated knockdown of endogenous RASSF1A or YAP was performed using Lipofectamine 2000 transfection reagent (Life Technologies, Inc.) and pre-designed pooled siRNAs (TriFECTa Kit, Integrated DNA Technologies) diluted in Opti-MEM (Gibco). GFP and scrambled siRNA CTRL (NC1, Negative Control Sequence) were used as controls, respectively.

Luciferase assay

Cells were transfected using Lipofectamine 2000 transfection reagent (Life Technologies, Inc.) according to the manufacturer's instructions. The NF-κB luciferase reporter gene p1242–3x-KB-L was purchased from Addgene (plasmid no. 26699) and was used to assess NF-κB activity (39). Following transfection, cells were lysed with Passive Lysis Buffer (Promega), and transcriptional activity was measured using the luciferase assay system (Promega) with an OPTOCOMP I luminometer (MGM instruments). All firefly luciferase results were normalized to total protein content as described previously (16, 40, 41).

Western blotting

For Western blotting, LV tissue or cells were homogenized in lysis buffer containing 50 mmol/liter Tris-HCl (pH 7.5), 150 mmol/liter NaCl, 1% IGEPAL CA-630, 0.1% SDS, 0.5% deoxycholic acid, 1 mmol/liter EDTA, 0.1 mmol/liter Na_3VO_4, 1 mmol/liter NaF, 50 μmol/liter phenylmethylsulfonyl fluoride (PMSF), 5 μg/ml aprotinin, and 5 μg/ml leupeptin. Following SDS-PAGE, Western blotting was performed using the following antibodies: RASSF1A (Abcam, ab23950, 1:1000); HA tag (Santa Cruz Biotechnology, sc-7392, 1:1000); glyceraldehyde-3-phosphate dehydrogenase (Cell Signaling Technology, 2118, 1:1000); phospho-Mst1 (Cell Signaling Technology, 3681, 1:1000); Mst1 (BD Biosciences, 611052, 1:1000); phospho-YAP (Cell Signaling Technology, 13008, 1:1000); YAP (Cell Signaling Technology, 14074, 1:1000); lamin AC (Cell Signaling Technology, 4777, 1:1000); RhoGDI (Santa Cruz Biotechnology, sc-360, 1:1000); IL-1β (Cell Signaling Technology, 12507, 1:1000); RelA (Cell Signaling Technology, 8242, 1:1000); α-tubulin (Sigma, T-6199, 1:1000); and α-actinin (Sigma, A-7811, 1:1000). Densitometry was performed using ImageJ software.

Quantitative PCR

Total RNA was isolated from cells or infarcted tissue using TRIzol (Life Technologies, Inc.); cDNA was generated using Moloney murine leukemia virus reverse transcriptase (Promega), and real-time quantitative PCR was performed using the PowerUp SYBR Green qPCR master mix (Applied Biosystems), as described previously (16). Primers (5′ to 3′) used to detect mouse sequences were as follows: *Tnfa*, CCCTCACACTCAGATCATCTTCT and GCTACGACGTGGGCTACAG; *Il-1b*, GCCCATCCTCTGTGACTCAT and AGGCCACAGGTATTTTGTCG; *Cox2*, TTCACCCGAGGACTGGGCCATGGA and GCCCCACAGCAAACTGCAGGTTCT; *Nos2*, GAGCGAGGAGCAGGTGGAAGACTA and GCGCTGCCCTTTTTTGCCCCATAG; *Arg1*, AGGCCCTGCAGCACTGAGGAA and GCCAGGTCCCCGTGGTCTCTCA; *Relm*, TGCCAATCCAGCTAACTATCC and GAGGCCCATCTGTTCATAGTC; *Ym1*, GAAGCCCTCCTAAGGACAAAC and GCAGCCTTGGAATGTCTTTCT; *Il-10*, CTCCTAGAGCTGCGGACTGCCTTCA and CTGGGGCATCACTTCTACCAGGTAAAA; *Il-12*, AGGTCACACTGGACCAAAGG and TGGTTTGATGTCCCTGA; *Ctgf*, CAAAGCAGCTGCAAATACCA and GGCCAAATGTGTCTTCCAGT; *Cyr61*, CAAGAAATGCAGCAAGACCA and GGAACCGCATCTTCACAGTT; *Tgfb1*, CTCCCGTGGCTTCTAGTGC and GCCTTAGTTTGGACAGGATCTG; *Col1a1*, GCTCCTCTTAGGGGCCACT and CCACGTCTCACCATTGGGG; *Col3a1*, CTGTAACATGGAAACTGGGGAAA and CCATAGCTGAACTGAAAACCACC; *Mmp2*, CAAGTTCCCCGGCGATGTC and TTCTGGTCAAGGTCACCTGTC; *Mmp9*, CTGGACAGCCAGACACTAAAG and CTCGCGGCAAGTCTTCAGAG; *Fn1*, ATGTGGACCCCTCCTGATAGT and GCCCAGTGATTTCAGCAAAGG; and *Rps15*, TTCGCAAGTTCACCTACC and CGGGCCGGCCATGCTTTA. Results were normalized to *Rps15* and relative quantitation was determined using the $\Delta\Delta C_T$ method (42).

Immunostaining

Mouse left ventricles were fixed in formalin and sectioned at 6-μm thickness. Tissue sections were then subjected to deparaffinization and antigen unmasking using citrate buffer and washed with PBS containing 0.3% Triton X-100. Samples were blocked with 5% BSA and incubated with primary antibody overnight and with Alexa Fluor 488- and Alexa Fluor 594–conjugated secondary antibodies (Molecular Probes) at room temperature. Primary antibodies used were anti-TNFα rabbit polyclonal antibody (Abcam), anti-F4/80 rat antibody (BioLegend), and anti-cardiac troponin-T mouse mAb (Thermo Fisher Scientific). Nuclei were stained with 4′,6-diamidino-2-phenylindole. Imaging was performed using a Nikon conventional fluorescence microscope.

Immunoprecipitation

Cell homogenates were prepared in lysis buffer containing 50 mmol/liter Tris-HCl (pH 7.5), 150 mmol/liter NaCl, 0.5% IGEPAL CA-630, 0.1% SDS, 0.5% deoxycholic acid, 1 mmol/liter EDTA, 0.1 mmol/liter Na_3VO_4, 1 mmol/liter NaF, 50 μmol/liter PMSF, 5 μg/ml aprotinin, and 5 μg/ml leupeptin. Samples were incubated with anti-FLAG (Cell Signaling Technology, 14793) or control IgG (Cell Signaling Technology, 2729) overnight at 4 °C, and immunocomplexes were precipitated following 1 h of incubation with protein A/G–agarose beads (Santa Cruz Biotechnology, sc-2003) (15).

Chromatin immunoprecipitation (ChIP)

ChIP assays were performed using the SimpleChIP Plus Enzymatic Chromatin IP kit (Cell Signaling) according to the manufacturer's instructions. Briefly, RAW264.7 cells were transduced with FLAG–YAP construct or control LacZ for 24 h, and then cells were cross-linked using 1% formaldehyde for 10 min. Cells were washed with 1× PBS, and glycine was added to stop the cross-linking reaction. Cells were then scraped; nuclei were isolated and lysed; and sheared chromatin was isolated after sonication. Immunoprecipitation reactions were carried out using chromatin extracts and anti-YAP (Cell Signaling Technology, 14074) or control IgG (Cell Signaling Technology, 2729) antibodies overnight at 4 °C. Equal amounts of purified input DNA was used to perform qPCR using primers specific to the promoters of the target genes. Primers (5′ to 3′) used for ChIP-qPCR were as follows: *Tnfα*, AGTGTTTAGGAGTGGGAGGGTG and GGAGCCTCTGCCATATCTTGACT; *IL-1β*, TGTTGTGAAATCAGTTAACCCAAGGGAA and GAGGATCCCAGATGAGCCTATTAG.

Nuclear fractionation

The nuclear and cytosolic-enriched fractions were prepared using NE-PER nuclear and cytoplasmic extraction kit (Pierce) according to the manufacturer's instructions (43). Western blotting was conducted following isolation of fractions.

TUNEL

DNA fragmentation was detected *in situ* using TUNEL as described previously (44). Heart sections were incubated with proteinase K, and DNA fragments were labeled with fluorescein-conjugated dUTP using TdT (Roche Applied Science), and cardiomyocytes were labeled using anti-cardiac troponin-T mouse mAb (Thermo Fisher Scientific, MA5-12960). TUNEL-positive cardiomyocyte nuclei (cardiac troponin-T-positive) were determined as a percentage of total cardiomyocyte nuclei.

ELISA

Following I/R and immediately prior to sacrifice, serum was collected, and the level of cardiac troponin-I was determined using the High Sensitivity Mouse Cardiac Troponin I ELISA according to the manufacturer's instructions (Life Diagnostics, Inc.). Ventricular tissue was homogenized, and TNFα protein was determined using a TNFα mouse ELISA kit according to the manufacturer's instructions (Thermo Fisher Scientific) (13).

Statistical analysis

All data are reported as mean ± S.E. of the mean. Student's *t* test was used to evaluate the difference in means between the two groups. One-way ANOVA was used to compare three or more group means with one independent variable. Two-way ANOVA was used to compare three or more group means with two independent variables. Post hoc comparisons were performed using Tukey's test. All mouse experiments used age-matched male mice and littermate controls and were performed blinded to genotype. Statistical analyses were performed using SPSS version 24 and Graph Pad Prism 6.0. A p value less than 0.05 was considered significant.

Author contributions—J. F., J. B., Y. Z., O. B. K., and S.-i. O. data curation; J. F., J. B., Y. Z., O. B. K., S.-i. O., and D. P. D. R. formal analysis; J. F., J. B., Y. Z., O. B. K., W. M., and P. Z. investigation; J. F., J. B., and D. P. D. R. writing-original draft; J. F., J. B., J. S., and D. P. D. R. writing-review and editing; J. S. and D. P. D. R. funding acquisition; J. S. and D. P. D. R. project administration; D. P. D. R. conceptualization.

Acknowledgments—We thank Dr. Louise van der Weyden for generously providing the RASSF1A mutant mice, and the New Jersey Medical School Flow Cytometry and Immunology Core for expert technical assistance.

References

1. Prabhu, S. D., and Frangogiannis, N. G. (2016) The biological basis for cardiac repair after myocardial infarction: from inflammation to fibrosis. *Circ. Res.* **119,** 91–112 CrossRef Medline
2. Frangogiannis, N. G. (2014) The inflammatory response in myocardial injury, repair, and remodelling. *Nat. Rev. Cardiol.* **11,** 255–265 CrossRef Medline
3. Tang, D., Kang, R., Coyne, C. B., Zeh, H. J., and Lotze, M. T. (2012) PAMPs and DAMPs: signal 0s that spur autophagy and immunity. *Immunol. Rev.* **249,** 158–175 CrossRef Medline
4. Mann, D. L. (2015) Innate immunity and the failing heart: the cytokine hypothesis revisited. *Circ. Res.* **116,** 1254–1268 CrossRef Medline
5. Swirski, F. K., and Nahrendorf, M. (2013) Leukocyte behavior in atherosclerosis, myocardial infarction, and heart failure. *Science* **339,** 161–166 CrossRef Medline
6. Frangogiannis, N. G., Dewald, O., Xia, Y., Ren, G., Haudek, S., Leucker, T., Kraemer, D., Taffet, G., Rollins, B. J., and Entman, M. L. (2007) Critical role of monocyte chemoattractant protein-1/CC chemokine ligand 2 in the

pathogenesis of ischemic cardiomyopathy. *Circulation* **115,** 584–592 CrossRef Medline
7. Courties, G., Heidt, T., Sebas, M., Iwamoto, Y., Jeon, D., Truelove, J., Tricot, B., Wojtkiewicz, G., Dutta, P., Sager, H. B., Borodovsky, A., Novobrantseva, T., Klebanov, B., Fitzgerald, K., Anderson, D. G., *et al.* (2014) *In vivo* silencing of the transcription factor IRF5 reprograms the macrophage phenotype and improves infarct healing. *J. Am. Coll. Cardiol.* **63,** 1556–1566 CrossRef Medline
8. O'Donoghue, M. L., Glaser, R., Cavender, M. A., Aylward, P. E., Bonaca, M. P., Budaj, A., Davies, R. Y., Dellborg, M., Fox, K. A., Gutierrez, J. A., Hamm, C., Kiss, R. G., Kovar, F., Kuder, J. F., Im, K. A., *et al.* (2016) Effect of losmapimod on cardiovascular outcomes in patients hospitalized with acute myocardial infarction: A randomized clinical trial. *JAMA* **315,** 1591–1599 CrossRef Medline
9. STABILITY Investigators, S., White, H. D., Held, C., Stewart, R., Tarka, E., Brown, R., Davies, R. Y., Budaj, A., Harrington, R. A., Steg, P. G., Ardissino, D., Armstrong, P. W., Avezum, A., Aylward, P. E., Bryce, A., *et al.* (2014) Darapladib for preventing ischemic events in stable coronary heart disease. *N. Engl. J. Med.* **370,** 1702–1711 CrossRef Medline
10. Ridker, P. M., Everett, B. M., Thuren, T., MacFadyen, J. G., Chang, W. H., Ballantyne, C., Fonseca, F., Nicolau, J., Koenig, W., Anker, S. D., Kastelein, J. J. P., Cornel, J. H., Pais, P., Pella, D., Genest, J., *et al.* (2017) Antiinflammatory therapy with canakinumab for atherosclerotic disease. *N. Engl. J. Med.* **377,** 1119–1131 CrossRef Medline
11. Dammann, R., Li, C., Yoon, J. H., Chin, P. L., Bates, S., and Pfeifer, G. P. (2000) Epigenetic inactivation of a RAS association domain family protein from the lung tumour suppressor locus 3p21.3. *Nat. Genet.* **25,** 315–319 CrossRef Medline
12. Grawenda, A. M., and O'Neill, E. (2015) Clinical utility of RASSF1A methylation in human malignancies. *Br. J. Cancer* **113,** 372–381 CrossRef Medline
13. Del Re, D. P., Matsuda, T., Zhai, P., Gao, S., Clark, G. J., Van Der Weyden, L., and Sadoshima, J. (2010) Proapoptotic Rassf1A/Mst1 signaling in cardiac fibroblasts is protective against pressure overload in mice. *J. Clin. Invest.* **120,** 3555–3567 CrossRef Medline
14. Oceandy, D., Pickard, A., Prehar, S., Zi, M., Mohamed, T. M., Stanley, P. J., Baudoin-Stanley, F., Nadif, R., Tommasi, S., Pfeifer, G. P., Armesilla, A. L., Cartwright, E. J., and Neyses, L. (2009) Tumor suppressor Ras-association domain family 1 isoform A is a novel regulator of cardiac hypertrophy. *Circulation* **120,** 607–616 CrossRef Medline
15. Del Re, D. P., Matsuda, T., Zhai, P., Maejima, Y., Jain, M. R., Liu, T., Li, H., Hsu, C. P., and Sadoshima, J. (2014) Mst1 promotes cardiac myocyte apoptosis through phosphorylation and inhibition of Bcl-xL. *Mol. Cell* **54,** 639–650 CrossRef Medline
16. Matsuda, T., Zhai, P., Sciarretta, S., Zhang, Y., Jeong, J. I., Ikeda, S., Park, J., Hsu, C. P., Tian, B., Pan, D., Sadoshima, J., and Del Re, D. P. (2016) NF2 activates Hippo signaling and promotes ischemia/reperfusion injury in the heart. *Circ. Res.* **119,** 596–606 CrossRef Medline
17. Nahrendorf, M., Swirski, F. K., Aikawa, E., Stangenberg, L., Wurdinger, T., Figueiredo, J. L., Libby, P., Weissleder, R., and Pittet, M. J. (2007) The healing myocardium sequentially mobilizes two monocyte subsets with divergent and complementary functions. *J. Exp. Med.* **204,** 3037–3047 CrossRef Medline
18. Hilgendorf, I., Gerhardt, L. M., Tan, T. C., Winter, C., Holderried, T. A., Chousterman, B. G., Iwamoto, Y., Liao, R., Zirlik, A., Scherer-Crosbie, M., Hedrick, C. C., Libby, P., Nahrendorf, M., Weissleder, R., and Swirski, F. K. (2014) Ly-6C high monocytes depend on Nr4a1 to balance both inflammatory and reparative phases in the infarcted myocardium. *Circ. Res.* **114,** 1611–1622 CrossRef Medline
19. Clausen, B. E., Burkhardt, C., Reith, W., Renkawitz, R., and Förster, I. (1999) Conditional gene targeting in macrophages and granulocytes using LysMcre mice. *Transgenic Res.* **8,** 265–277 CrossRef Medline
20. Gordon, M., El-Kalla, M., Zhao, Y., Fiteih, Y., Law, J., Volodko, N., Anwar-Mohamed, A., El-Kadi, A. O., Liu, L., Odenbach, J., Thiesen, A., Onyskiw, C., Ghazaleh, H. A., Park, J., Lee, S. B., *et al.* (2013) The tumor suppressor gene, RASSF1A, is essential for protection against inflammation-induced injury. *PLoS ONE* **8,** e75483 CrossRef Medline
21. Schmidt, M. L., Hobbing, K. R., Donninger, H., and Clark, G. J. (2018) RASSF1A deficiency enhances RAS-driven lung tumorigenesis. *Cancer Res.* **78,** 2614–2623 CrossRef Medline
22. Taniguchi, K., and Karin, M. (2018) NF-κB, inflammation, immunity and cancer: coming of age. *Nat. Rev. Immunol.* **18,** 309–324 CrossRef Medline
23. Honold, L., and Nahrendorf, M. (2018) Resident and monocyte-derived macrophages in cardiovascular disease. *Circ. Res.* **122,** 113–127 CrossRef Medline
24. Epelman, S., Lavine, K. J., Beaudin, A. E., Sojka, D. K., Carrero, J. A., Calderon, B., Brija, T., Gautier, E. L., Ivanov, S., Satpathy, A. T., Schilling, J. D., Schwendener, R., Sergin, I., Razani, B., Forsberg, E. C., *et al.* (2014) Embryonic and adult-derived resident cardiac macrophages are maintained through distinct mechanisms at steady state and during inflammation. *Immunity* **40,** 91–104 CrossRef Medline
25. Lavine, K. J., Epelman, S., Uchida, K., Weber, K. J., Nichols, C. G., Schilling, J. D., Ornitz, D. M., Randolph, G. J., and Mann, D. L. (2014) Distinct macrophage lineages contribute to disparate patterns of cardiac recovery and remodeling in the neonatal and adult heart. *Proc. Natl. Acad. Sci. U.S.A.* **111,** 16029–16034 CrossRef Medline
26. Hulsmans, M., Clauss, S., Xiao, L., Aguirre, A. D., King, K. R., Hanley, A., Hucker, W. J., Wulfers, E. M., Seemann, G., Courties, G., Iwamoto, Y., Sun, Y., Savol, A. J., Sager, H. B., Lavine, K. J., *et al.* (2017) Macrophages facilitate electrical conduction in the heart. *Cell* **169,** 510–522.e20 CrossRef Medline
27. Heidt, T., Courties, G., Dutta, P., Sager, H. B., Sebas, M., Iwamoto, Y., Sun, Y., Da Silva, N., Panizzi, P., van der Lahn, A. M., Swirski, F. K., Weissleder, R., and Nahrendorf, M. (2014) Differential contribution of monocytes to heart macrophages in steady-state and after myocardial infarction. *Circ. Res.* **115,** 284–295 CrossRef Medline
28. Bajpai, G., Bredemeyer, A., Li, W., Zaitsev, K., Koenig, A. L., Lokshina, I., Mohan, J., Ivey, B., Hsiao, H. M., Weinheimer, C., Kovacs, A., Epelman, S., Artyomov, M., Kreisel, D., and Lavine, K. J. (2019) Tissue resident CCR2− and CCR2+ cardiac macrophages differentially orchestrate monocyte recruitment and fate specification following myocardial injury. *Circ. Res.* **124,** 263–278 CrossRef Medline
29. Dick, S. A., Macklin, J. A., Nejat, S., Momen, A., Clemente-Casares, X., Althagafi, M. G., Chen, J., Kantores, C., Hosseinzadeh, S., Aronoff, L., Wong, A., Zaman, R., Barbu, I., Besla, R., Lavine, K. J., *et al.* (2019) Self-renewing resident cardiac macrophages limit adverse remodeling following myocardial infarction. *Nat. Immunol.* **20,** 29–39 CrossRef Medline
30. Swirski, F. K., and Nahrendorf, M. (2018) Cardioimmunology: the immune system in cardiac homeostasis and disease. *Nat. Rev. Immunol.* **18,** 733–744 CrossRef Medline
31. van der Weyden, L., Tachibana, K. K., Gonzalez, M. A., Adams, D. J., Ng, B. L., Petty, R., Venkitaraman, A. R., Arends, M. J., and Bradley, A. (2005) The RASSF1A isoform of RASSF1 promotes microtubule stability and suppresses tumorigenesis. *Mol. Cell. Biol.* **25,** 8356–8367 CrossRef Medline
32. Agah, R., Frenkel, P. A., French, B. A., Michael, L. H., Overbeek, P. A., and Schneider, M. D. (1997) Gene recombination in postmitotic cells. Targeted expression of Cre recombinase provokes cardiac-restricted, site-specific rearrangement in adult ventricular muscle *in vivo*. *J. Clin. Invest.* **100,** 169–179 CrossRef Medline
33. Sadoshima, J., and Izumo, S. (1993) Molecular characterization of angiotensin II-induced hypertrophy of cardiac myocytes and hyperplasia of cardiac fibroblasts: a critical role of the AT1 receptor subtype. *Circ. Res.* **73,** 413–423 CrossRef Medline
34. Yamamoto, S., Yang, G., Zablocki, D., Liu, J., Hong, C., Kim, S. J., Soler, S., Odashima, M., Thaisz, J., Yehia, G., Molina, C. A., Yatani, A., Vatner, D. E., Vatner, S. F., and Sadoshima, J. (2003) Activation of Mst1 causes dilated cardiomyopathy by stimulating apoptosis without compensatory ventricular myocyte hypertrophy. *J. Clin. Invest.* **111,** 1463–1474 CrossRef Medline
35. Raschke, W. C., Baird, S., Ralph, P., and Nakoinz, I. (1978) Functional macrophage cell lines transformed by Abelson leukemia virus. *Cell* **15,** 261–267 CrossRef Medline
36. Chen, B., Huang, S., Su, Y., Wu, Y. J., Hanna, A., Brickshawana, A., Graff, J., and Frangogiannis, N. G. (2019) Macrophage Smad3 protects the in-

farcted heart, stimulating phagocytosis and regulating inflammation. *Circ. Res.* 125, 55–70 CrossRef Medline

37. Ortiz-Vega, S., Khokhlatchev, A., Nedwidek, M., Zhang, X. F., Dammann, R., Pfeifer, G. P., and Avruch, J. (2002) The putative tumor suppressor RASSF1A homodimerizes and heterodimerizes with the Ras-GTP binding protein Nore1. *Oncogene* **21,** 1381–1390 CrossRef Medline
38. Zhao, B., Wei, X., Li, W., Udan, R. S., Yang, Q., Kim, J., Xie, J., Ikenoue, T., Yu, J., Li, L., Zheng, P., Ye, K., Chinnaiyan, A., Halder, G., Lai, Z. C., and Guan, K. L. (2007) Inactivation of YAP oncoprotein by the Hippo pathway is involved in cell contact inhibition and tissue growth control. *Genes Dev.* **21,** 2747–2761 CrossRef Medline
39. Mitchell, T., and Sugden, B. (1995) Stimulation of NF-κB–mediated transcription by mutant derivatives of the latent membrane protein of Epstein-Barr virus. *J. Virol.* **69,** 2968–2976 Medline
40. Yang, Y., Del Re, D. P., Nakano, N., Sciarretta, S., Zhai, P., Park, J., Sayed, D., Shirakabe, A., Matsushima, S., Park, Y., Tian, B., Abdellatif, M., and Sadoshima, J. (2015) miR-206 mediates YAP-induced cardiac hypertrophy and survival. *Circ. Res.* **117,** 891–904 CrossRef Medline
41. Ikeda, S., Mizushima, W., Sciarretta, S., Abdellatif, M., Zhai, P., Mukai, R., Fefelova, N., Oka, S. I., Nakamura, M., Del Re, D. P., Farrance, I., Park, J. Y., Tian, B., Xie, L. H., Kumar, M., *et al.* (2019) Hippo deficiency leads to cardiac dysfunction accompanied by cardiomyocyte dedifferentiation during pressure overload. *Circ. Res.* **124,** 292–305 CrossRef Medline
42. Matsuda, T., Jeong, J. I., Ikeda, S., Yamamoto, T., Gao, S., Babu, G. J., Zhai, P., and Del Re, D. P. (2017) H-Ras isoform mediates protection against pressure overload-induced cardiac dysfunction in part through activation of AKT. *Circ. Heart Fail.* **10,** e003658 CrossRef Medline
43. Byun, J., Del Re, D. P., Zhai, P., Ikeda, S., Shirakabe, A., Mizushima, W., Miyamoto, S., Brown, J. H., and Sadoshima, J. (2019) Yes-associated protein (YAP) mediates adaptive cardiac hypertrophy in response to pressure overload. *J. Biol. Chem.* **294,** 3603–3617 CrossRef Medline
44. Del Re, D. P., Yang, Y., Nakano, N., Cho, J., Zhai, P., Yamamoto, T., Zhang, N., Yabuta, N., Nojima, H., Pan, D., and Sadoshima, J. (2013) Yes-associated protein isoform 1 (Yap1) promotes cardiomyocyte survival and growth to protect against myocardial ischemic injury. *J. Biol. Chem.* **288,** 3977–3988 CrossRef Medline